Robust Circadian Oscillations in Growing Cyanobacteria Require Transcriptional Feedback

Supplementary Materials for
Robust circadian oscillations in growing cyanobacteria require transcriptional feedback

Shu-Wen Teng[1], Shankar Mukherji[1]*, Jeffrey R. Moffitt[2]*, Sophie de Buyl[3]*, Erin K. O'Shea[1]†

†To whom correspondence should be addressed. E-mail: erin_oshea@harvard.edu

This PDF file includes:

Materials and Methods
Supplementary Text
Figs. S1 to S10
Tables S1
References (27-38)

Materials and Methods

Strain Construction

PTR-only strain

To investigate the role of the TTR, we generated a PTR-only strain in which transcriptional feedback of *kaiBC* is abrogated. To construct this strain, we used microarray data to identify genes whose expression does not oscillate or whose expression is out of phase with the expression of the *kaiBC* promoter, and we used RNA-Seq data to identify genes with the similar mean expression level to that of the *kaiBC* gene *(27, 28)*. We found four genes that satisfied these criteria: hypothetical proteins *synpcc7942_0004*, *synpcc7942_0050*, *synpcc7942_0607*, and *synpcc7942_2513*. We cloned the predicted promoters (with lengths from 400 bp to 700 bp) for these genes into plasmid pAM1580 between the XmaI and StuI sites in front of a gene encoding a bioluminescent reporter *(29)*. These constructs were then incorporated into neutral site I on the chromosome in *S. elongatus* using homologous recombination *(30)*. Expression was evaluated using a TopCount machine to measure bioluminescence. For comparison, we placed the bioluminescent reporter under the control of the *kaiBC* promoter. We selected candidate promoters that have similar mean expression output to that of the *kaiBC* promoter, but whose expression does not oscillate as a function of circadian time. We identified the best two candidates: 700bp upstream of the translation start of *synpcc7942_0050* and 400bp upstream of *synpcc7942_0607*, and constructed two corresponding PTR-only candidates: ST09 and ST35. We started with JRC35 *(21)*, which contains the gene encoding a YFP-SsrA reporter protein whose expression is driven by the *kaiBC* promoter at neutral site II. We deleted the endogenous *kaiBC* locus in this strain to create ST07. We constructed two strains in which expression of the *kaiBC* operon was driven by one of the two candidate promoters introduced into neutral site I in the ST07 background using plasmid pAM1303. We used Western blotting to quantify the KaiC concentration for these two PTR-only candidates. We found that KaiC is expressed constitutively in the ST09 PTR-only strain, and the expression level is higher than the trough of the WT oscillation (Fig. S1A).

To confirm that the observed desynchronization of the PTR-only strain is a consequence of the loss of TTR and not of incorrect levels of KaiC, we created a strain in which the KaiC level could be controlled by IPTG (Fig. S1E) *(31)*. In the IPTG-inducible strain, we deleted the endogenous *kaiBC* locus, and the *kaiBC* operon was driven by P_{trc} promoter introduced into neutral site I. We find that the KaiC expression level with 6 μM IPTG, monitored by Western blotting, is similar to the average KaiC expression of the WT strain (Fig. S1A). Under these conditions, a population of cells of this strain desynchronized in 2.5 days (Fig. S1B and S1C). In agreement with previous findings *(11)*, we observed that the KaiBC expression level is not truly constitutive for the IPTG-inducible promoter (Fig. S1A). Our observation that desynchronization occurs in the IPTG-inducible strain confirms that the desynchronization is not a consequence of a low KaiC expression level and also indicates that desynchronization is observed with only a partial abrogation of TTR.

TTR-only strain

To evaluate the contribution of PTR to circadian oscillations, we studied a TTR-only strain in which the PTR has been abrogated through mutation of KaiC phosphorylation sites. To generate this strain we first deleted the endogenous *kaiBC* genes in the background in which the YFP-SsrA protein is driven by the *kaiBC* promoter as a reporter at neutral site II. We then created a mutant KaiC in which residues S431 and T432 were replaced with glutamic acid (the mutant is referred to as KaiC EE) using a QuikChange II XL Site-Directed Mutagenesis Kit (Agilent Technologies). A similar mutant strain has been analyzed previously at the population level in bulk culture *(9, 14)*. The KaiC EE mutant was introduced into the *kaiBC* operon driven by the *kaiBC* promoter and introduced into neutral site I using plasmid pAM1303.

We used Western blotting to quantify the KaiC concentration for the WT and TTR-only strains. The cell cultures were entrained for two cycles of twelve hour light and dark pulses before time zero and the Western blot measurement was conducted at the 30 hour time point. This time point corresponds to the plateau in KaiC expression level for the TTR-only strain (Fig. 3B), and the mean expression level for the WT strain (Fig. 2A). We find that the KaiC expression levels are similar between the two strains (Fig. S6C).
To understand the cause of the initial dip in the fluorescence of the expression reporter in the TTR-only strain (Fig. 3B), we performed our standard microfluidics measurement but introduced a dark pulse 12 hours after the cells were loaded into the microfluidics device. We find that the TTR-only strain responds to 12-hour dark pulse with a dip right after pulse application (Fig. S6D), suggesting that the dip is the consequence of the dark pulse response, but not a consequence of the perturbation caused by culture transfer to the microfluidics device.

Western blot analysis

Cell pellets containing 4.5 OD_{750} units of cells were lysed in 100 µl of lysis buffer (7.5 M urea, 20 mM HEPES pH 8.0, 1 mM DTT, 1x Roche EDTA-free Complete protease inhibitor tablet). The resuspended cells were lysed by bead-beating, the lysate was cleared by centrifugation, and the supernatant was transferred to a 96-well plate. The protein concentration of each sample was measured by BCA assay (Pierce) using BSA (Bio-Rad) diluted into lysis buffer as the standard. Normalized samples for Western blot analysis were prepared by combining 4 µg of lysate, 6x SDS-PAGE sample buffer, and fresh lysis buffer to a final volume of 12 µl. Standards consisting of a dilution series of recombinant protein in lysis buffer were included in each gel. The proteins were transferred from the 4-20% gel to a nitrocellulose membrane (Protran). The membrane was blocked in 2.5% milk in TBST buffer (50 mM Tris, 150 mM NaCl, 0.1% Tween-20, pH 7.6.), incubated in primary antibody (1:5000 dilution of affinity-purified polyclonal α-KaiC) diluted into 2.5% milk in TBST. The membrane was washed and incubated with secondary antibody (1:2500 dilution of 10µg/ml goat anti-rabbit HRP conjugate (Pierce)) diluted into 2.5% milk in TBST. The blot was developed with the SuperSignal West Femto kit (Pierce). The protein abundance was quantified by comparing the Western blot signal to the recombinant protein standards. The absolute concentration of KaiC was determined from the number of cells per ml per OD_{750} measured by Multisizer 3 Coulter

Counter (Beckman) and from the 4 fl average cell volume estimated from phase contrast images.

Culture Preparation before Microscopy

Cultures of *S. elongatus* were grown in BG-11M *(32)* liquid medium with shaking (150 rpm) and continuous illumination (see Illumination and Growth Rate for details) at 30°C to OD_{750} of 0.3 to 0.4. Samples (Fig. 1, Fig. 2, Fig. 3, Fig. S1, Fig. S3, Fig. S4, Fig. S6B, Fig. S7, Fig. S9) were entrained for two cycles of twelve hour light and dark pulses before time zero of the measurement. Samples in Fig. S6D were exposed to continuous illumination without entrainment before the measurement. For single cell measurements, 1 ml of cell culture was concentrated by centrifugation and resuspended into 50 µl of medium. 1.5 µl of concentrated cell culture (~10^5 cells) was loaded into the microfluidics device (Fig. S2).

Microscopy Experimental Setup

An automated AxioObserver Z1 inverted microscope (Zeiss) was used for the long-term time lapse single cell measurements. The YFP was excited by a Colibri LED module 505 nm (Zeiss). Images were collected with a 200 ms exposure time every 20 minutes. Both the fluorescence and phase images were measured with a Plan-Apochromat 100X/1.40 Oil Ph3 objective (Zeiss) with the fluorescence filter set 46 HE YFP. The digital images were recorded by an Evolve EMCCD Camera (Photometric). The microscope was maintained at 30°C by an XL-S1 incubator system and a heat insert (Lab-TekTM S1). The microfluidics device was custom made and assembled as previous described *(23)*. A range of track widths and depths were tested with *S. elongatus,* and 1.2-µm deep tracks with widths ranging from 0.5-0.9 µm were found to best constrain the growth of this bacterium into linear colonies. The agarose pads used for all reported data contained tracks of three different widths, 0.5, 0.6, and 0.7 µm, and two lengths, 50 or 100 µm. It was found that, unlike *E. coli (23)*, pressure from compression of the agarose pad within the device could inhibit growth of *S. elongatus*. To relieve this compression, the top coverslip was sealed onto the device with fast dry epoxy rather than with the typical polydimethylsiloxane-glass bond *(23)*. To prevent the formation of air bubbles during prolonged measurements with the microfluidics device, BG-11M liquid medium was equilibrated above 30°C for 2 days before measurement to allow excess dissolved gas to effervesce out of the medium. This medium was then injected into the microfluidics chamber at 30°C with a Harvard Apparatus Model 11 Syringe Pump (Instech Laboratories). See Fig. S2 for a schematic of the setup.

Illumination and Growth Rate

On the microscope, the external LED ring (Advanced Illumination) was controlled by an LED controller box (Advanced Illumination) and a trigger board (PCI xPress; Zeiss). The external LED illuminated samples between every two image acquisitions, and the external LED switched off during the image acquisition. The intensity of illumination was ~25 µE m^{-2} s^{-1} for high growth rate WT and PTR-only samples in Fig. S4 with an average doubling time of 14-16 hours, and TTR-only sample in Fig. S7 with an average doubling time of 6 hours. The intensity of illumination was ~10 µE m^{-2} s^{-1} for low growth

rate WT and PTR-only samples (Fig.2) with an average doubling time of 72 hours, and TTR-only sample in Fig. 3 with an average doubling time of 24 hours.

	WT strain	PTR-only	TTR-only
high growth rate	16 hours	14 hours	6 hours
low growth rate	72 hours	72 hours	24 hours

Image Processing and Data Analysis

Image processing and data analysis were performed with custom software written in Matlab (MathWorks). The image analysis algorithm is described in Moffitt et al. *(23)*. Single-cell lineages were extracted from the phase contrast images (Fig. S9). The yellow fluorescence intensity from individual cell lineages was quantified accordingly using a moving average filter with a span of 8 data points. Multiple micro-colonies were measured to generate a population ensemble. (e.g. 38 micro-colonies in WT strain Fig. 2A). The average fluorescence intensity of the population was fit with a cosine function to identify the period of the ensemble (Fig. S9B). The amplitude and phase were extracted from individual fluorescence lineages (Fig. S9C). As a result, the distribution of amplitude and phase in a population was a function of time, and the polar plots in Fig. 2B and 2D show the distribution of amplitude and phase at day 1 and day 4. The amplitude distribution does not change with time in five days and is similar to previous findings *(4)*. The phase distribution changed with time in the PTR-only strain and was quantified by the synchronization index as described below.

Synchronization Index Definition

To characterize the strength of synchronization in our data we quantified the measured phase distributions according to Tass et al. *(24)*. These authors introduce the synchronization index which is based on the Shannon entropy of the phase distribution. It is defined as $SI = (S_{\max} - S)/S_{\max}$, where $S = -\sum_{k=1}^{N} p_k \ln p_k$ is the entropy of the distribution. $S_{\max} = \ln N$, where N is the number of bins, and p_k is the probability of data occurrence in each bin. Normalized in this way, $0 \le SI \le 1$, where $SI = 1$ corresponds to perfect synchronization and $SI = 0$ corresponds to no synchronization. We calculated the histogram of the phase distribution as a function of time with 8 bins. To test the sensitivity of the synchronization index to the number of bins, we quantified the synchronization index for the ensemble of individual cells as a function of time with different bin numbers. Fig. S10 shows that the SI does not depend strongly on the bin size. Using the bootstrapping method, we calculated the standard deviation of the samples to generate error bars for the synchronization index (Fig. 2E, 4F, S1C, S4G, and S4H, S9). This sampling method draws 100 bootstrap data samples, computes statistics on each sample using the definition of synchronization index, and returns the data samples for error quantification.

Supplemental Text

Quantifying the degree of synchronization

We quantified the phase dispersion of the WT strain using two approaches. First, we used a previously described method *(4)* and find that correlation time is 78 ± 40 days, shorter than the measurement previous reported 166 ± 100 days *(4)*. This discrepancy may result from differences in experimental conditions. Previous work used a bioluminescent reporter that required signal integration over a substantial period of time *(4)*. As a result the cells were exposed to a dark environment for 30 min every 2 hours. In our experiment, the cells were exposed to a dark environment for 1 min every 20 min. Second, we calculated the synchronization index *(24)*. We selected this metric for two reasons: (1) first, the synchronization index can be accurately calculated at any time point and thus does not require a long time series; and (2) the synchronization index calculation does not make any any assumption regarding the mathematical process underlying phase dispersion. By contrast, the correlation time calculation is based on the assumption that phase dispersion is governed by the Wiener process (random walk) *(4)*. For these reasons, we used synchronization index to quantify the degree of synchronization and present this metric in the main text of the manuscript.

Mathematical model for the *in vivo* oscillator

Our model of the WT circuit is built on the models of the TTR-only and PTR-only circuits. The model of the TTR-only circuit is based on a simple negative feedback loop. The model of PTR-only circuit is based on the *in vitro* model described previously *(7)* with addition of terms for production, degradation, and dilution of KaiC.

Model of the TTR-only circuit

For the TTR-only strain, we model KaiC as being present only in its ST-form (doubly-phosphorylated; variable C in the equation) because the mutations of phosphorylation sites to glutamate (E) lock it in a state that mimics phosphorylation *(9, 14)*. Regulation is provided by autorepression of the production of *kaiC* mRNA (variable M term in the equation) production. The dependence of M on C is represented with a Hill function characterized by a degree of cooperativity n and the threshold constant for repression K_i. The rate of translation of M into C is governed by a rate of synthesis characterized by an apparent first-order rate constant K_s. Active degradation of C and M are modeled by Michaelis-Menten degradation terms with maximal rates V and V_m respectively, and Michaelis constants K and K_m respectively *(25)*. Dilution due to cell division affected C and was modeled by a linear degradation term V_d. We did not include a dilution term for M because its active degradation rate is much faster than the dilution rate.

$$\frac{dM}{dt} = V_s \cdot \frac{K_i^n}{K_i^n + C^n} - V_m \cdot \frac{M}{K_m + M} \quad (1)$$

$$\frac{dC}{dt} = K_s \cdot M - V \cdot \frac{C}{K + C} - V_d \cdot C \quad (2)$$

Model of the PTR-only circuit

The model of the PTR-only circuit is based on the *in vitro* model described previously *(7)*. To adapt this model to the *in vivo* case, we added terms for production (K_s), and degradation (V) and dilution (V_d) rates. We assume that all phosphorylated forms of KaiC have the same linear dilution rate (V_d) and Michaelis-Menten degradation rate (V, K). For mRNA, we add Michaelis-Menten degradation terms (V_m, K_m) without a dilution term, as above. Newly synthesized KaiC appears first in its unphosphorylated form; thus, we add a production term, K_s, for the unphosphorylated form of KaiC. Since there is no transcriptional or translational regulation in the PTR-only circuit, we modeled the production of mRNA with a constant rate V_{sptr}. The equations are given by

$$\frac{dU}{dt} = k_{TU} \cdot T + k_{SU} \cdot S - k_{UT} \cdot U - k_{US} \cdot U - V \cdot \frac{U}{K + U} - V_d \cdot U + K_s \cdot M \quad (3)$$

$$\frac{dT}{dt} = k_{UT} \cdot U + k_{DT} \cdot D - k_{TU} \cdot T - k_{TD} \cdot T - V \cdot \frac{T}{K + T} - V_d \cdot T \quad (4)$$

$$\frac{dD}{dt} = k_{TD} \cdot T + k_{SD} \cdot S - k_{DT} \cdot D - k_{DS} \cdot D - V \cdot \frac{D}{K + D} - V_d \cdot D \quad (5)$$

$$\frac{dS}{dt} = k_{US} \cdot U + k_{DS} \cdot D - k_{SU} \cdot S - k_{SD} \cdot S - V \cdot \frac{S}{K + S} - V_d \cdot S \quad (6)$$

$$\frac{dM}{dt} = V_{sptr} - V_m \cdot \frac{M}{K_m + M} \quad (7)$$

Where U, T, D, S are the concentrations of U-KaiC (unphosphorylated KaiC), T-KaiC (KaiC phosphorylated only on threonine), ST-KaiC (KaiC phosphorylated on both serine and threonine), and S-KaiC (KaiC phosphorylated only on serine), respectively. The parameter k_{XY} depends on S and is therefore time-dependent *(7)*,

$$k_{XY} = k_{XY}^0 + \frac{k_{XY}^A \cdot A(S)}{K_{1/2} + A(S)} \quad (8)$$

$$A(S) = \max\left[0, KaiA - 2S\right] \quad (9)$$

The values of the concentration of KaiA causing a half-maximal effect on KaiC's autokinase rates $(K_{1/2})$, rate constant for conversion of KaiC phosphoform x to y in the absence of KaiA (k_{XY}^0), and rate constant for conversion of KaiC phosphoform x to y in the maximal influence of KaiA (k_{XY}^A) are the same as in the *in vitro* model *(7)*.

Model of the WT circuit

To model the WT circuit with both forms of regulation, we combined equations (1), (3), (4), (5), (6), and adapted the production rate of mRNA to be dependent on all forms of KaiC. The only parameters left to fit to the experimental data were the coefficients

c_U, c_T, c_D, and c_S - these parameters determine how *kaiBC* transcription is repressed by each of the four phosphorylated forms of KaiC.

$$\frac{dU}{dt} = k_{TU} \cdot T + k_{SU} \cdot S - k_{UT} \cdot U - -k_{US} \cdot U - V \cdot \frac{U}{K + U} - V_d \cdot U + K_s \cdot M \quad (10)$$

$$\frac{dT}{dt} = k_{UT} \cdot U + k_{DT} \cdot D - k_{TU} \cdot T - k_{TD} \cdot T - V \cdot \frac{T}{K + T} - V_d \cdot T \quad (11)$$

$$\frac{dD}{dt} = k_{TD} \cdot T + k_{SD} \cdot S - k_{DT} \cdot D - k_{DS} \cdot D - V \cdot \frac{D}{K + D} - V_d \cdot D \quad (12)$$

$$\frac{dS}{dt} = k_{US} \cdot U + k_{DS} \cdot D - k_{SU} \cdot S - k_{SD} \cdot S - V \cdot \frac{S}{K + S} - V_d \cdot S \quad (13)$$

$$\frac{dM}{dt} = V_s \cdot \frac{K_i^n}{K_i^n + C_r^n} - V_m \cdot \frac{M}{K_m + M} \quad (14)$$

$$C_r = c_U \cdot U + c_T \cdot T + c_D \cdot D + c_S \cdot S \quad (15)$$

Parameters for Simulation

We performed least squares fitting to derive parameters for the TTR-only model from our experimental data in Fig. 3E. Thus, the parameters for the models of the TTR-only circuit and the PTR *in vitro* circuit *(7)* are obtained from experimental measurement. V_{sptr} is the only tunable parameter in the PTR-only *in vivo* model, and c_U, c_T, c_D, c_S are the only four tunable parameters in the WT model. We scanned over a wide range of these five parameters. Based on our experimental results in Fig. 2, we selected values of the parameters which generate sustained oscillations for both the PTR-only model and WT model. The values of c_U, c_T, c_D, c_S from scanning of the model suggest that *kaiBC* expression is regulated primarily by the S-KaiC and U-KaiC phosphoforms. This result is now supported by new data from our laboratory *(33)* .

The initial condition for these simulations was selected by selecting parameters constrained by experimental observations. The total initial KaiC concentration is ~3.8 μM, as measured by Western blotting (Fig. S1A). The ratio of the four different phosphorylated forms of KaiC initial concentration was based on the *in vitro* measurements of the ratio *(7)*. The simulations were performed using the algorithm of *(26)* written in Matlab (MathWorks).

Model Simplification

The simplified WT and PTR models (Fig. 4) do not produce oscillations as stable as those observed in Fig. 2. We reason that this discrepancy is due to simplifications of the PTR circuit and simplification of the coupling between the TTR and PTR – both simplifications are made because we cannot experimentally constrain more complex models. The PTR circuit based on the *in vitro* model *(7)* neglects the existence of KaiC as a hexamer *(34)*. The *in vitro* PTR model does not describe the monomer exchange between hexamers *(35)* that has the potential to increase the tendency of the system to oscillate *(36)*. We used a simple negative feedback loop to describe the function of the TTR circuit and neglect the details of the molecular mechanism. The TTR circuit is

complex, involving two component signaling transduction *(37)*, supercoiling *(28)*, and chromosome compaction *(38)*. Even with these simplifications, our model demonstrates that the WT circuit is more stable than the PTR circuit.

Sensitivity Analysis

To study the response of the oscillatory dynamics of the PTR-only and WT circuits to parameter changes, we integrated the differential equations making up each model for many parameter sets. We paid particular attention to those parameters that are likely sources of stochastic fluctuations in single cyanobacterial cells: kinetic rates and concentrations of regulators like KaiA.

General Approach

For each set of parameters under study, we numerically solved the WT and PTR models for at least the equivalent of 720 hours (or 30 days) to allow sufficient discrimination between sustained and damped oscillations, using the ode45 routine in MATLAB. For the PTR model at extremely low dilution and, thus, long relaxation times, we equilibrated the model for ~180 days. We used the same experimentally motivated initial conditions as used in the stochastic simulations above. Generically there are 3 types of trajectories in the simulations: i) non-oscillatory, ii) damped oscillations, and iii) sustained oscillations. By Fourier transforming each trace, we produce a power spectrum that contain three pieces of information that we can use to distinguish these cases: peak position, peak height, and peak width (or linewidth). To distinguish true sustained oscillations from damped oscillations and non-oscillatory trajectories, we followed the standard technique of subtracting the mean, or DC component, of the trajectory, computing the power spectral density via Fourier transforming the trajectory, and locating the tallest peak in the power spectrum. We found that setting a threshold peak height on the tallest peak could already at this stage distinguish between trajectories exhibiting sustained oscillations from those that did not; Fourier peaks above the threshold very reliably mapped onto trajectories with sustained oscillations. We set the threshold to be half the height of the dominant Fourier peak in the WT system. The location of the dominant Fourier peak was identified as the frequency of the trajectory. We then determined whether this frequency falls within +/- 5 hours around the circadian frequency of the WT system, and if it does classify the oscillation as circadian. We selected +/- 5 hours because the same relative range of frequencies is observed in the measured WT system power spectrum in Fig. 3C. We then plot this oscillation classification as a function of the parameters that are scanned over (Figs. 4G, H, S8)

To ensure that we were not throwing away small amplitude sustained oscillations, however, we also extracted the linewidth of the dominant peak by fitting the peak to a Gaussian function (or Lorentzian; our results were insensitive to choice of fitting function) and labeling parameter sets that produced linewidths smaller than a threshold width to be oscillatory. We set the threshold linewidth to be twice the width of the dominant Fourier peak in the WT system. The linewidth is a very sensitive indicator of whether the oscillation is sustained or not as oscillation damping, even if subtle, will markedly broaden the width of the Fourier peak. In practice, however, the linewidth criterion did not alter the classification obtained from examining the peak heights alone.

It should be noted that we also repeated the classification by examining the turning points of the trajectories and noted whether they: i) existed—if they did not then the trajectory was labeled non-oscillatory—or ii) maintained a constant, positive value with time, if they did then the trajectory was labeled oscillatory. This analysis gave the same result as the Fourier analysis detailed above.

Simultaneously varying the KaiC translation and dilution rates

Perhaps the most important parameters to vary and understand the resulting effects on the dynamics of the WT and PTR-only systems are those related to production and decay of KaiC protein, because these parameters play a major role in determining the quantity that is regulated by the TTR system – the overall cellular KaiC abundance – and are likely sources of stochastic fluctuations in single cyanobacterial cells. By varying the production and decay parameters in the WT and PTR-only systems and extracting the resulting dynamics, we can isolate any impact that TTR has on buffering the oscillator against processes that change KaiC abundance.

To carry out the simulations, we chose dilution to represent the decay processes and KaiC translation to represent the production process; we achieved very similar results when choosing to vary the KaiC degradation or *kaiBC* mRNA transcription rates. The rates were chosen according to the following table:

Parameter	Min value	Max value	Spacing
K_s	0.05	106	logarithmic
V_d	$2\text{x}10^{-4}$	0.43	logarithmic

For each (V_d, K_s) pair, we followed the procedure detailed in the General Approach above and plotted whether the model produced circadian oscillations, non-circadian oscillations, or no oscillations for both the WT and PTR-only systems (Fig. 4G, H). The simulations indicate that the PTR-only system exhibits circadian oscillations in a very limited parameter space. The WT system, on the other hand, exhibits circadian oscillations in a far larger volume of parameter space than the PTR-only system. The fraction of the (V_d, K_s) parameter space swept by the simulations that support circadian and non-circadian oscillations are listed in the table below.

System	% circadian oscillations	% non-circadian oscillations
WT	20.0%	22.6%
PTR-only	1.4%	0.5%

Simultaneously modulating the TTR feedback strength and parameters common to WT and PTR-only systems

To quantitatively evaluate the importance of the TTR negative feedback in buffering the oscillator against variation in other kinetic rates that are likely sources of stochastic fluctuations in single cyanobacterial cells, we simultaneously varied kinetic rate constants common to the WT and PTR-only circuits, systematically tuned the TTR feedback

strength and performed numerical simulations for every parameter choice. The values of the parameters scanned over are listed in the table below.

Parameter	Min value	Max value	Spacing
K_s	0.05	106	logarithmic
V_d	$2\text{x}10^{-4}$	0.43	logarithmic
V_m	$5\text{x}10^{-3}$	7.89	logarithmic
V	$2\text{x}10^{-4}$	0.31	logarithmic

To tune the negative feedback strength from TTR, we scanned through logarithmically spaced values of the *kaiBC* transcriptional saturation constant K_I from 0.1 to 1000. We chose this method of tuning the feedback by observing that when K_I is large compared to the scaled concentration of KaiC, KaiC cannot effectively inhibit *kaiBC* transcription, thus weakening the feedback strength. In order to keep the mean levels of KaiC comparable between different TTR feedback strengths, we adjusted the value of the transcription rate V_s for each choice of K_I with $K_I = 1000$, representing the PTR-only system, simulated with $V_s = V_{sptr}$. For each choice of kinetic rate and K_i we repeated our sensitivity analysis. The results of this are depicted in Fig. S8. Additionally, in the tables below, we present the fraction of the values scanned over for a given parameter that give rise to circadian and non-circadian oscillations at a given value of K_I. For example, in the case of K_s, the table shows that when $K_I = 1$, 29.63% of all K_s values scanned generate circadian oscillations in the simulations, while 30.86% of all K_s values generate non-circadian oscillations; the remaining 39.51% of K_s values yield no oscillations. In general, we see that as the TTR feedback strength is turned down, the space of parameters supporting circadian oscillations decreases for variations in every kinetic rate.

Scanning over K_s

K_I	% circadian oscillations	% non-circadian oscillations
0.1	0%	0%
1 (WT)	29.63%	30.86%
10	2.47%	3.7%
100	2.47%	2.47%
1000 (~PTR-only)	2.47%	2.47%

Scanning over V_d

K_I	% circadian oscillations	% non-circadian oscillations
0.1	0%	0%
1 (WT)	62.96%	1.23%
10	4.94%	3.7%
100	4.94%	2.47%
1000 (~PTR-only)	4.94%	2.47%

Scanning over V_m

K_I	% circadian oscillations	% non-circadian oscillations
0.1	0%	0%
1 (WT)	27.16%	19.75%

10	2.47%	2.47%
100	2.47%	1.23%
1000 (~PTR-only)	2.47%	1.23%

Scanning over V

K_I	% circadian oscillations	% non-circadian oscillations
0.1	0%	0%
1 (WT)	64.20%	1.23%
10	8.64%	17.28%
100	7.41%	12.35%
1000 (~PTR-only)	7.41%	12.35%

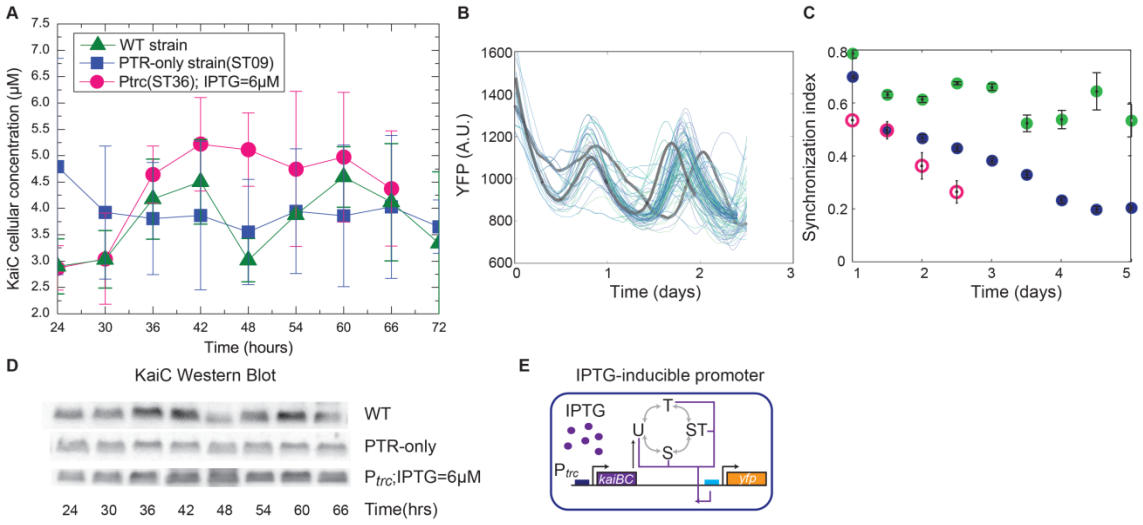

Fig. S1. Strain construction and characterization of the PTR-only strain. (**A**) KaiC protein expression level characterized by quantitative Western blotting. Strains were entrained for 2 days before time zero and then exposed to constant light for three days with the measurement starting at 24 hours. The WT strain (green) and PTR-only strain (blue) were used to generate Figures 1 and 2A-D. KaiC expression level oscillates with a period of 24 hours in the WT strain, while KaiC is expressed constitutively in the PTR-only strain with the level slightly higher than the trough of the KaiC level in the WT strain. The strain expressing IPTG-inducible *kaiBC* expresses KaiC at levels higher than the mean level of WT, with residual circadian dependence. The error bars are from duplicates of the Western blots. (**B**) Fluorescence intensity of IPTG-inducible strain grown with 6 μM IPTG (~160 cell lineages). Two traces are randomly picked and highlighted in black. (**C**) Synchronization index for the ensemble of individual cells as a function of time for low growth rate (average doubling time of 72 hours) of the WT (green filled circle), PTR-only (blue filled circle), and IPTG-inducible strains (pink empty circle). (**D**) Representative Western blots of the WT strain (upper panel), PTR-only strain (middle panel), and IPTG-inducible strain (lower panel). (**E**) The genetic circuit of the IPTG-inducible promoter strain. To study if desynchronization is a consequence of a KaiC expression level lower than the average in the WT strain, we created an IPTG-inducible strain in which *kaiBC* expression is driven by an IPTG-inducible promoter (pink symbols and line in (A)). The KaiC expression level with 6μM IPTG is similar to the average KaiC expression of the WT strain, but has residual circadian dependence.

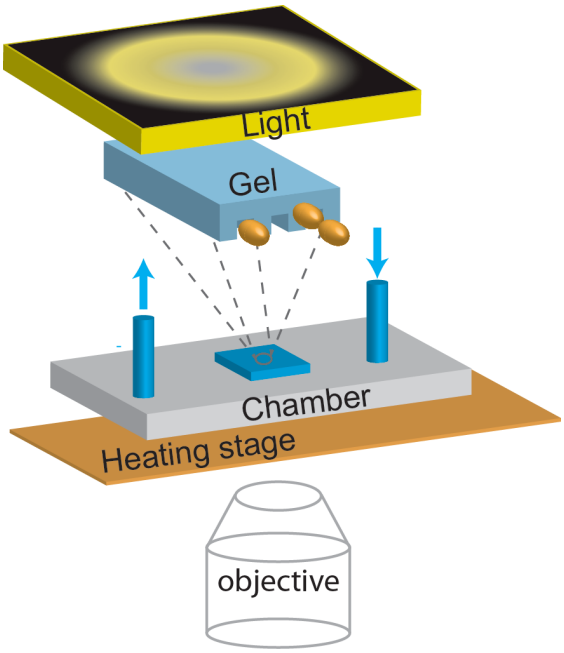

Fig. S2. Microfluidics device and microscopy set up. The chemostatic environment is created by the microfluidics device. The LED light ring array (top square) controls the light intensity for the growth of *S. elongatus*. The spatial intensity distribution of light was shown to be uniform in the field of view (data not shown). The microfluidics chamber (middle rectangular in gray) is sandwiched between the LED light and the heating stage. The inlet tubing is connected to a syringe pump containing BG-11 medium, and the outlet tubing is connected to a waste container. A nano-patterned agarose pad is in the center of the chamber (middle square in blue) to direct the growth of linear colonies of *S. elongatus*. The metal heating stage (bottom rectangular in brown) directly contacts the bottom of the chamber, and the whole microscope is maintained at 30°C to reduce thermal fluctuations.

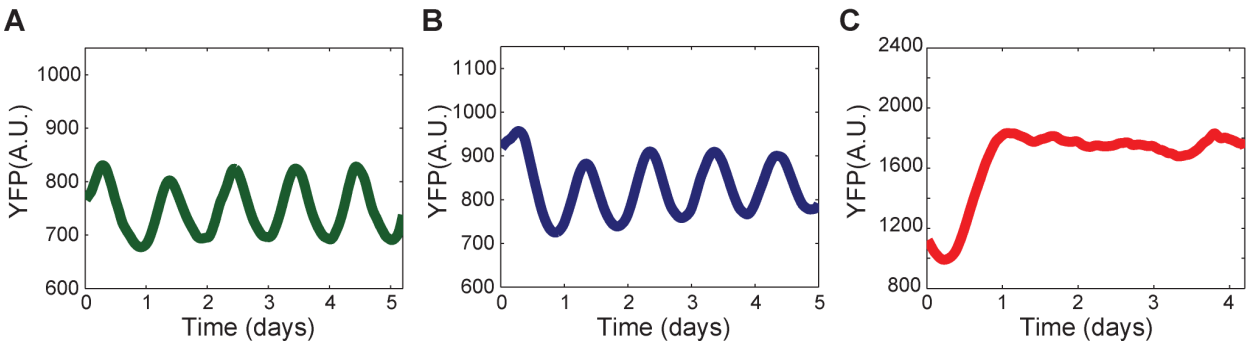

Fig. S3. Population averages of single cell data. (**A**) The population average of the WT strain shown in Figure 2A. The amplitude of the population oscillation remains constant for five days. (**B**) The population average of the PTR-only strain shown in Figure 2C. (**C**) The population average of the TTR-only strain shown in Figure 3B.

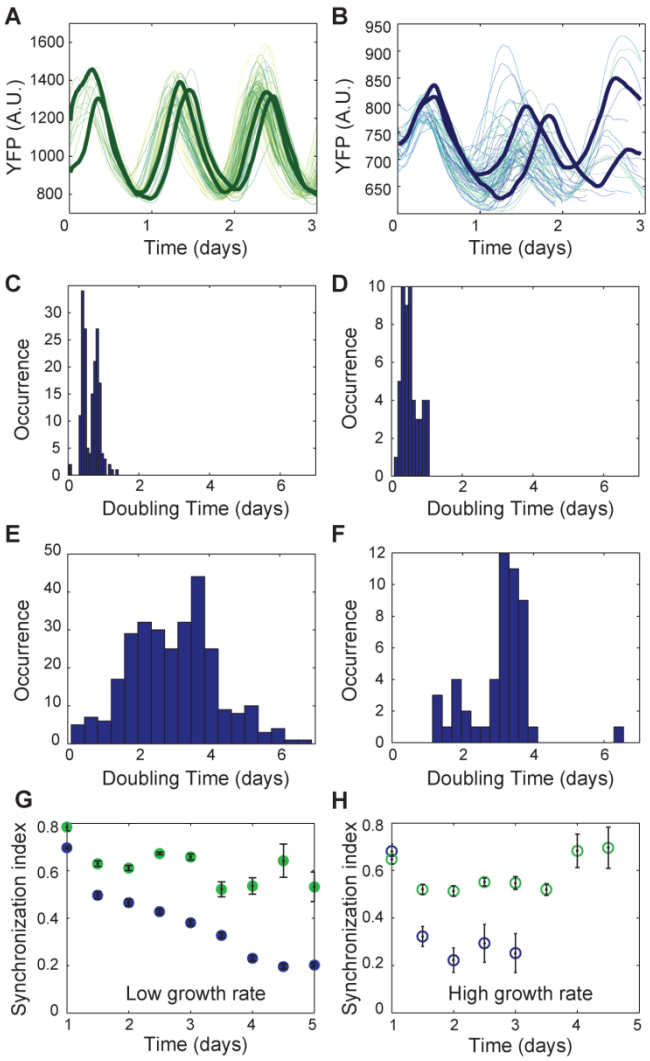

Fig. S4. Transcriptional feedback regulation is required to maintain population synchrony at higher growth rate. (**A**) Fluorescence intensity of WT cells at high growth rate (~230 cell lineages). Two traces are randomly selected and highlighted in dark green. (**B**) Fluorescence intensity of PTR-only cells at high growth rate (~130 cell lineages). Two traces are randomly selected and highlighted in dark blue. (**C**) The histogram of the doubling time of the WT cells at high growth rate (average doubling time of 16 hours). (**D**) The histogram of the doubling time of the PTR-only cells at high growth rate (average doubling time of 14 hours). (**E**) The histogram of the doubling time of WT cells (Figure 2A) at low growth rate (average doubling time of 72 hours). (**F**) The histogram of the doubling time of PTR-only cells (Figure 2C) at low growth rate (average doubling time of 72 hours). (**G**) Synchronization index for the ensemble of individual cells as a function of time for low growth rate of the WT (green empty circle) and the PTR-only (blue empty circle) strains, and for high growth rate of the WT (green filled circle) and the PTR-only (blue filled circle) strains.

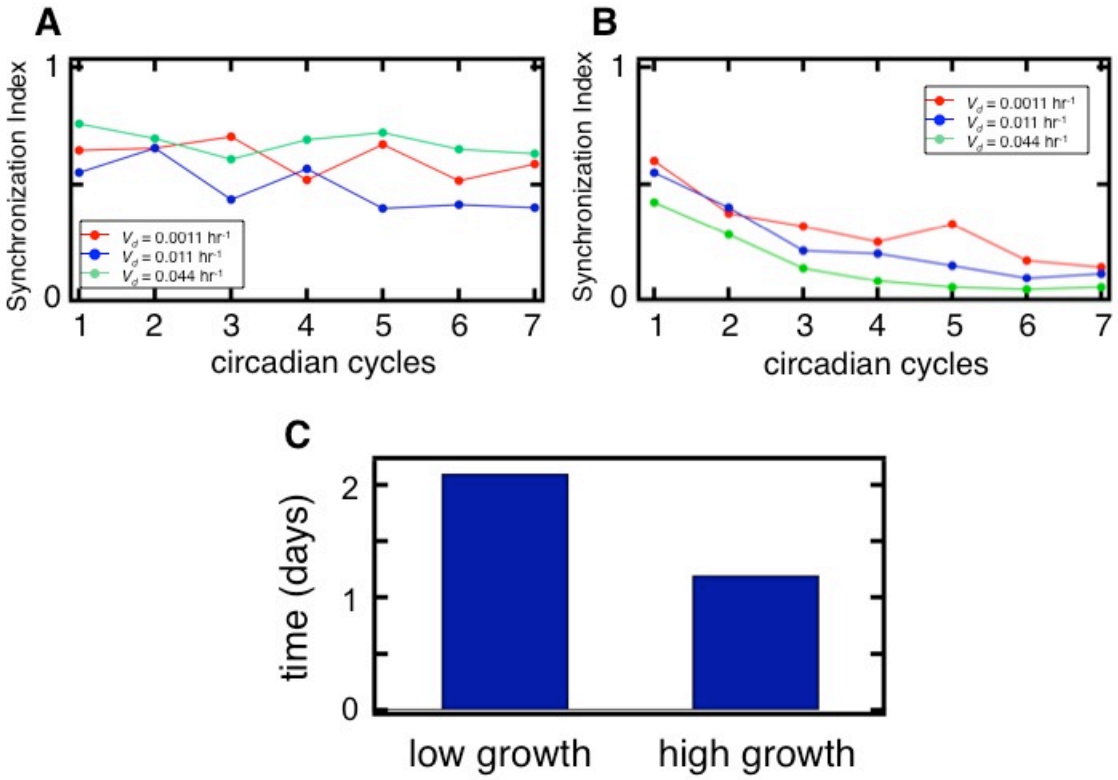

Fig. S5. Theoretical prediction of accelerated decay of SI in PTR-only system as a function of growth rate. **(A)** The SI as a function of circadian cycles in the simulated WT system for a series of growth rates as modeled by changing dilution rates V_d. **(B)** The SI as a function of circadian cycles as in (A) but for the PTR-only system. **(C)** The time taken for the SI of the PTR-only strain to decay to half the WT value for low (V_d = 0.0011 hr^{-1}) and high (V_d = 0.044 hr^{-1}) growth conditions.

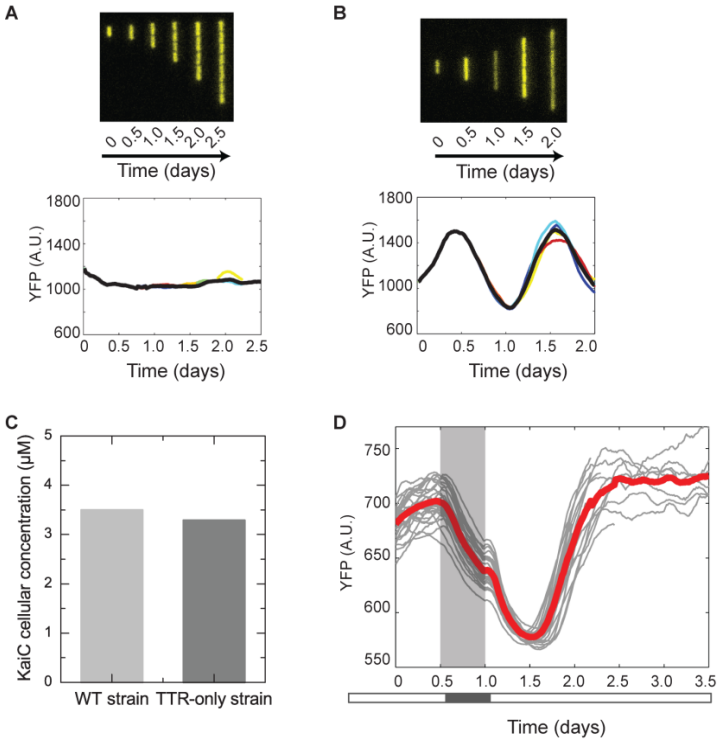

Fig. S6. Strain construction of the TTR-only strain. (**A**) The *ΔkaiBC* strain was generated by deleting the *kaiBC* operon on the chromosome, and one *yfp* reporter driven by the *kaiBC* promoter was introduced into neutral site II on the chromosome. At the single-cell level, the fluorescence reporter is expressed constitutively with no oscillations (upper panel). The expression level is constant for two and half days (lower panel) indicating that the pacemaker is abrogated in individual cells. (**B**) Introduction of the *kaiBC* operon driven by *kaiBC* promoter into neutral site I on the chromosome of the *ΔkaiBC* strain restores oscillations in yfp expression. The double mutant KaiC$^{S431E/T432E}$ was introduced into the *kaiBC* locus in place of WT KaiC to create the TTR-only strain. (**C**) Western blot analysis of the WT strain and TTR-only strain demonstrates that the KaiC expression levels are similar. The cell cultures were entrained for two cycles of twelve hour light and dark entrainment before time zero and the Western blot measurement was conducted at the 30 hour time point, which corresponds to the plateau of KaiC expression in Figure 3B for the TTR-only strain, and the mean expression level of the WT strain. (**D**) We confirmed that the initial dip in YFP expression in the single-cell traces of the TTR-only strain (Figure 3B) is not due to the initial perturbation of transferring cells to the microfluidics device and assembling the chamber. Without two days of entrainment before the measurement (the light environment is indicated by the white-dark bar below x-axis), the TTR-only strain responds to a 12-hour dark pulse with a dip in YFP expression. This dip is similar to the initial dip in Figure 3B, suggesting that it is a consequence of the dark pulse response and not a result of other environmental perturbations.

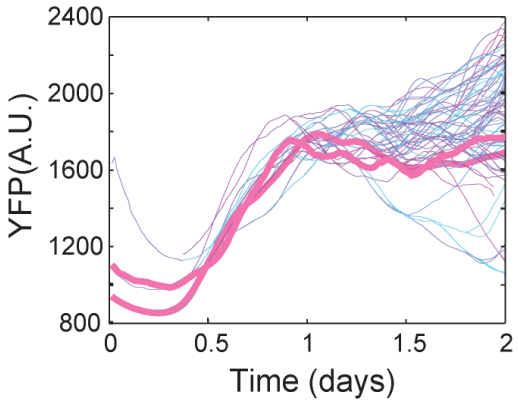

Fig. S7. Fluorescence intensity derived from the circadian reporter measured in individual cell lineages of the TTR-only strain at high growth rate (average doubling time of 6 hours) for 2 days. Two single-cell traces are randomly selected and highlighted in pink.

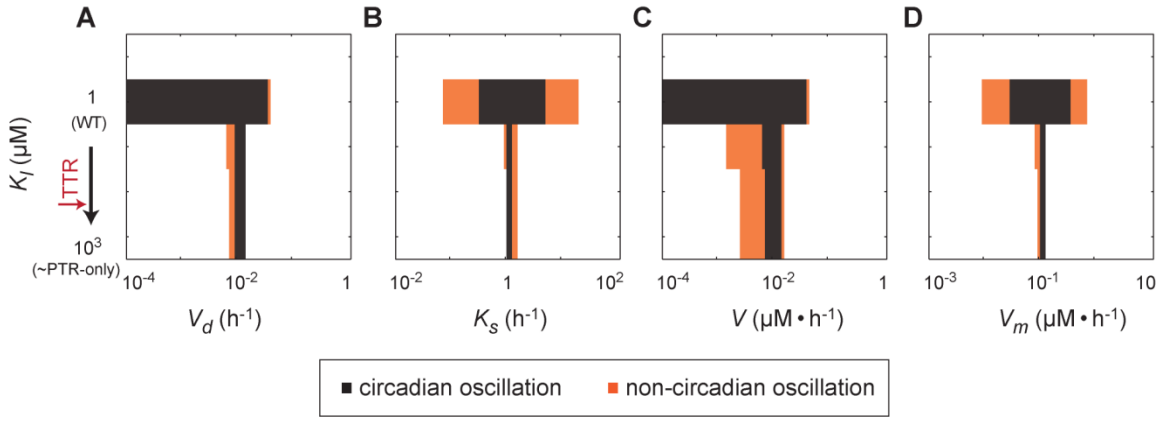

Fig. S8. Simulating the effect of TTR negative feedback strength on robustness of the circadian oscillator. We performed sensitivity analyses on the circadian oscillator frequency by simultaneously varying the saturation constant K_I, thereby tuning the strength of the TTR negative feedback, and the **(A)** dilution rate V_d, **(B)** translation rate K_s, **(C)** KaiC protein degradation rate V, **(D)** *kaiBC* mRNA degradation rate V_m. For a given choice of the parameter under study and K_I, we first classify whether the solution to the model oscillates or not and if it does, we further classify whether it oscillates with circadian period (marked in black) or non-circadian period (marked in orange).

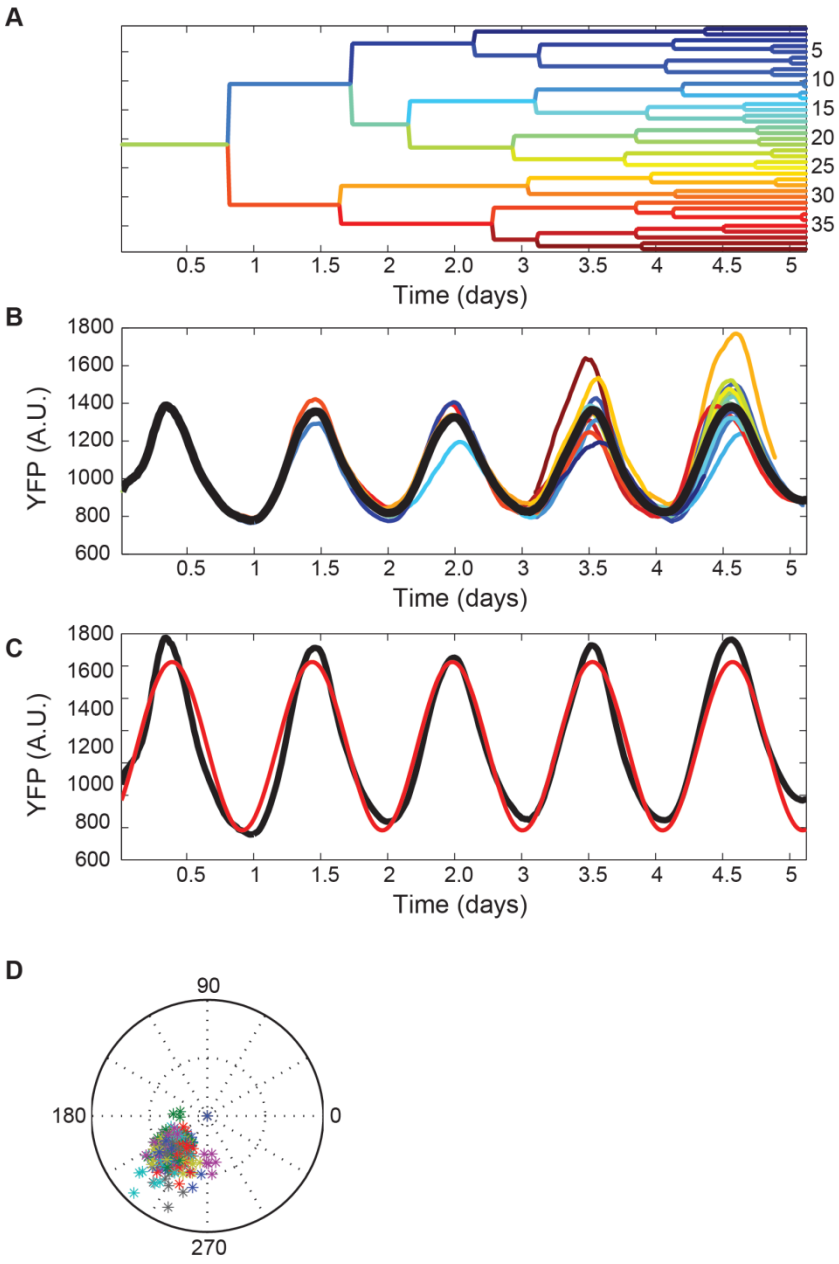

Fig. S9. Image processing and data analysis. (**A**) The single-cell lineage is extracted from the time-lapse WT strain images in Figure 1C. (**B**) The yellow fluorescence intensity (total photon/cell area) is quantified for each individual cell. (**C**) The average fluorescence intensity (black line) of the population is fitted with a cosine function (red line) to identify the period. 72 data points from each day of individual cell traces in (B) are fitted with this fixed period to extract the amplitude and phase for individual cellular lineages. (**D**) The polar plot shows the amplitude (radius axis) and the phase (angular axis) of individual cellular lineages in the WT strain grown for five days.

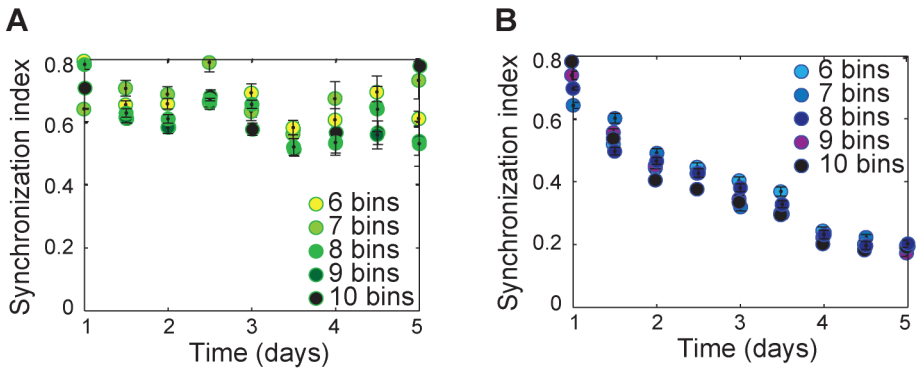

Fig. S10. Synchronization index for the ensemble of individual cells as a function of time with different bin numbers. The phases, ranging from 0 to 2π, are equally divided into 6 to 10 bins. In Fig. 2E and 4F, synchronization index is calculated using 8 bins. (**A**) Synchronization index for the WT strain with different bin numbers. (**B**) Synchronization index for the PTR-only strain with different bin numbers. The slopes of the synchronization index functions are not changed with the change in the bin numbers.

Table S1.

Category	Process	Parameter Name	Value	Experiment
TTR-only	mRNA production	Vs KI n	$2\ \mu M \cdot h^{-1}$ $1\ \mu M$ 4	Figure 3
	mRNA degradation	Vm Km	$0.2\ \mu M \cdot h^{-1}$ $0.2\ \mu M$	
	KaiC production	Ks	$2.7\ h^{-1}$	
	KaiC degradation	V K	$0.0078\ \mu M \cdot h^{-1}$ $0.1\ \mu M$	
	KaiC dilution	Vd	$0.022\ h^{-1}$	
PTR-only	T → U (Basal Rates)	k_{TU}^{0}	$0.21\ h^{-1}$	Based on previous *in vitro* model *(7)*
	D → T (Basal Rates)	k_{DT}^{0}	$0\ h^{-1}$	
	D → S (Basal Rates)	k_{DS}^{0}	$0.031\ h^{-1}$	
	S → U (Basal Rates)	k_{SU}^{0}	$0.11\ h^{-1}$	
	U → T (KaiA effect)	k_{UT}^{A}	$0.479\ h^{-1}$	
	T → D (KaiA effect)	k_{TD}^{A}	$0.213\ h^{-1}$	
	S → D (KaiA effect)	k_{SD}^{A}	$0.5057\ h^{-1}$	
	U → S (KaiA effect)	k_{US}^{A}	$0.0532\ h^{-1}$	
	T → U (KaiA effect)	k_{TU}^{A}	$0.0798\ h^{-1}$	
	D → T (KaiA effect)	k_{DT}^{A}	$0.173\ h^{-1}$	
	D → S (KaiA effect)	k_{DS}^{A}	$-0.32\ h^{-1}$	
	S → U (KaiA effect)	k_{SU}^{A}	$-0.133\ h^{-1}$	
	Concentration of KaiA causing half-maximal effect on KaiC	$K_{1/2}$	$0.43\ \mu M$	
	mRNA production	$Vsptr$	$0.03316\ \mu M \cdot h^{-1}$	Figure 2
WT	Transcriptional regulation	c_U c_T c_D c_S	0.9 0.5 0.3 1	Figure 2
Simulation	Initial condition	U^0 T^0 D^0 S^0 M^0	$2.23\ \mu M$ $0.83\ \mu M$ $0.31\ \mu M$ $0.48\ \mu M$ $0.037\ \mu M$	Total [KaiC] from Fig. S1A; phosphoforms based on *in vitro* measurements *(7)*

Parameters used in the model shown in above equations. The experimental data from which the parameter was determined is listed in the right-most column. The initial conditions used in the simulations shown in Figure 4A-D are listed at the bottom of the table (see Parameters for Simulation for details).

Supplemental References

1. J. C. Dunlap, J. J. Loros, P. J. Decoursey, J. C. Dunlap, J. J. Loros, Chronobiology: Biological timekeeping. *Chronobiology: Biological Timekeeping.*, i-xx, 1-406 (2004).

2. S. L. Harmer, S. Panda, S. A. Kay, Molecular bases of circadian rhythms. *Annu. Rev. Cell Dev. Biol.* **17**(2001).

3. J. C. Dunlap, Molecular bases for circadian clocks. *Cell.* **96**(1999).

4. I. Mihalcescu, W. H. Hsing, S. Leibler, Resilient circadian oscillator revealed in individual cyanobacteria. *Nature.* **430**, 81-85 (2004).

5. M. Amdaoud, M. Vallade, C. Weiss-Schaber, I. Mihalcescu, Cyanobacterial clock, a stable phase oscillator with negligible intercellular coupling. *Proc. Natl. Acad. Sci. U. S. A.* **104**, 7051-7056 (2007).

6. J. Tomita, M. Nakajima, T. Kondo, H. Iwasaki, No transcription-translation feedback in circadian rhythm of KaiC phosphorylation. *Science.* **307**, 251-254 (2005).

7. M. J. Rust, J. S. Markson, W. S. Lane, D. S. Fisher, E. K. O'Shea, Ordered phosphorylation governs oscillation of a three-protein circadian clock. *Science.* **318**, 809-812 (2007).

8. J. S. Markson, E. K. O'Shea, The molecular clockwork of a protein-based circadian oscillator. *FEBS Lett.* **583**, 3938-3947 (2009).

9. X. M. Qin, M. Byrne, Y. Xu, T. Mori, C. H. Johnson, Coupling of a Core Post-Translational Pacemaker to a Slave Transcription/Translation Feedback Loop in a Circadian System. *Plos Biology.* **8**(2010).

10. M. Ishiura *et al.*, Expression of a gene cluster kaiABC as a circadian feedback process in cyanobacteria. *Science.* **281**, 1519-1523 (1998).

11. Y. Nakahira *et al.*, Global gene repression by KaiC as a master process of prokaryotic circadian system. *Proc. Natl. Acad. Sci. U. S. A.* **101**, 881-885 (2004).

12. M. W. Young, S. A. Kay, Time zones: A comparative genetics of circadian clocks. *Nature Reviews Genetics.* **2**(2001).

13. M. Gallego, D. M. Virshup, Post-translational modifications regulate the ticking of the circadian clock. *Nat. Rev. Mol. Cell Biol.* **8**, 139-148 (2007).

14. Y. Kitayama, T. Nishiwaki, K. Terauchi, T. Kondo, Dual KaiC-based oscillations constitute the circadian system of cyanobacteria. *Genes Dev.* **22**, 1513-1521 (2008).

15. J. S. O'Neill, A. B. Reddy, Circadian clocks in human red blood cells. *Nature.* **469**, 498-U70 (2011).

16. J. S. O'Neill *et al.*, Circadian rhythms persist without transcription in a eukaryote. *Nature.* **469**, 554-558 (2011).

17. M. Nakajima *et al.*, Reconstitution of circadian oscillation of cyanobacterial KaiC phosphorylation in vitro. *Science.* **308**, 414-415 (2005).

18. D. Zwicker, D. K. Lubensky, P. R. ten Wolde, Robust circadian clocks from coupled protein-modification and transcription-translation cycles. *Proc. Natl. Acad. Sci. U. S. A.* **107**, 22540-22545 (2010).

19. N. Hosokawa *et al.*, Circadian transcriptional regulation by the posttranslational oscillator without de novo clock gene expression in Synechococcus. *Proc. Natl. Acad. Sci. U. S. A.* **108**, 15396-15401 (2011).

20. Y. Xu, T. Mori, C. H. Johnson, Cyanobacterial circadian clockwork: roles of KaiA, KaiB and the kaiBC promoter in regulating KaiC. *EMBO J.* **22**(2003).

21. J. R. Chabot, J. M. Pedraza, P. Luitel, A. van Oudenaarden, Stochastic gene expression out-of-steady-state in the cyanobacterial circadian clock. *Nature.* **450**, 1249-1252 (2007).

22. Q. Yang, B. F. Pando, G. Dong, S. S. Golden, A. van Oudenaarden, Circadian Gating of the Cell Cycle Revealed in Single Cyanobacterial Cells. *Science.* **327**(2010).

23. J. R. Moffitt, J. B. Lee, P. Cluzel, The single-cell chemostat: an agarose-based, microfluidic device for high-throughput, single-cell studies of bacteria and bacterial communities. *Lab on a Chip.* **12**(2012).

24. P. Tass *et al.*, Detection of n : m phase locking from noisy data: Application to magnetoencephalography. *Phys. Rev. Lett.* **81**(1998).

25. D. Gonze, J. Halloy, A. Goldbeter, Robustness of circadian rhythms with respect to molecular noise. *Proc. Natl. Acad. Sci. U. S. A.* **99**(2002).

26. D. T. Gillespie, Exact Stochastic Simulation of Coupled Chemical-Reactions. *J. Phys. Chem.* **81**(1977).

27. V. Vijayan, I. H. Jain, E. K. O'Shea, A high resolution map of a cyanobacterial transcriptome. *Genome Biol.* **12**, R47 (2011).

28. V. Vijayan, R. Zuzow, E. K. O'Shea, Oscillations in supercoiling drive circadian gene expression in cyanobacteria. *Proc. Natl. Acad. Sci. U. S. A.* **106**, 22564-22568 (2009).

29. S. R. Mackey, J. L. Ditty, E. M. Clerico, S. S. Golden, Detection of rhythmic bioluminescence from luciferase reporters in cyanobacteria. *Methods Mol. Biol.* **362**(2007).

30. E. M. Clerico, J. L. Ditty, S. S. Golden, Specialized techniques for site-directed mutagenesis in cyanobacteria. *Methods Mol. Biol.* **362**(2007).

31. Y. Murayama, T. Oyama, T. Kondo, Regulation of circadian clock gene expression by phosphorylation states of KaiC in cyanobacteria. *J. Bacteriol.* **190**(2008).

32. S. A. Bustos, S. S. Golden, Expression of the Psbdii Gene in Synechococcus Sp Strain-Pcc-7942 Requires Sequences Downstream of the Transcription Start Site. *J. Bacteriol.* **173**(1991).

33. A. Gutu, E. K. O'Shea, Two antagonistic clock-regulated histidine kinases time the activation of circadian gene expression. *In Press.*

34. T. Mori *et al.*, Circadian clock protein KaiC forms ATP-dependent hexameric rings and binds DNA. *Proc. Natl. Acad. Sci. U. S. A.* **99**(2002).

35. H. Kageyama *et al.*, Cyanobacterial circadian pacemaker: Kai protein complex dynamics in the KaiC phosphorylation cycle in vitro. *Mol. Cell.* **23**(2006).

36. E. Emberly, N. S. Wingreen, Hourglass model for a protein-based circadian oscillator. *Phys. Rev. Lett.* **96**, 038303 (2006).

37. N. Takai *et al.*, A KaiC-associating SasA-RpaA two-component regulatory system as a major circadian timing mediator in cyanobacteria. *Proc. Natl. Acad. Sci. U. S. A.* **103**(2006).

38. R. M. Smith, S. B. Williams, Circadian rhythms in gene transcription imparted by chromosome compaction in the cyanobacterium Synechococcus elongatus. *Proc. Natl. Acad. Sci. U. S. A.* **103**, 8564-8569 (2006).